PRESSURE AND CURRENT EFFECTS ON THE THERMAL EFFICIENCY OF AN MPD ARC USED AS A PLASMA SOURCE

Thomas J. Pivirotto

July 10, 1972

Backup Document for AIAA Synoptic Scheduled

for Publication in the AIAA Journal, January 1973

Jet Propulsion Laboratory
California Institute of Technology
4800 Oak Grove Drive
Pasadena, California 91103

SYNOPTIC BACKUP DOCUMENT

This document is made publicly available through the NASA scientific and technical information system as a service to readers of the corresponding "Synoptic" which is scheduled for publication in the following (checked) technical journal of the American Institute of Aeronautics and Astronautics.

- [XXX] AIAA Journal, January 1973
- [ ] Journal of Aircraft
- [ ] Journal of Spacecraft & Rockets
- [ ] Journal of Hydronautics

A Synoptic is a brief journal article that presents the key results of an investigation in text, tabular, and graphical form. It is neither a long abstract nor a condensation of a full length paper, but is written by the authors with the specific purpose of presenting essential information in an easily assimilated manner. It is editorially and technically reviewed for publication just as is any manuscript submission. The author must, however, also submit a full backup paper to aid the editors and reviewers in their evaluation of the synoptic. The backup paper, which may be an original manuscript or a research report, is not required to conform to AIAA manuscript rules.

For the benefit of readers of the Synoptic who may wish to refer to this backup document, it is made available in this microfiche (or facsimile) form without editorial or makeup changes.

#

Pressure and Current Effects on the Thermal Efficiency of an MPD Arc Used as a Plasma Source*

Thomas J. Pivirotto†

Jet Propulsion Laboratory, Pasadena, California

Abstract

Measurements of arc voltage and energy loss to the cooled electrodes of a magnetoplasmadynamic (MPD) arc, operating without an applied magnetic field, were made at chamber pressures of 26 to 950 torr, argon mass flow rates of 0.08 to 44 g/s and current of 200 to 2000 A. The resulting arc thermal efficiency varied from 22% at a chamber pressure of 26 torr to 88% at 950 torr. Thermal efficiency was only weakly dependent on arc current. It is concluded that the MPD arc operating without an applied magnetic field and at higher pressure than normally used in thruster applications is a reliable and efficient steady-state plasma source.

---

*This work presents the results of one phase of research carried out in the Propulsion Research and Advanced Concepts Section of the Jet Propulsion Laboratory, California Institute of Technology, under Contract No. NAS 7-100, sponsored by the National Aeronautics and Space Administration.

The author is grateful to Gary Russell of the Jet Propulsion Laboratory for his advice and encouragement.

Index Categories: Plasma Dynamics and MHD; Research Facilities and Instrumentation; Electric and Advanced Space Propulsion.

†Senior Engineer.

I. Introduction

There has been considerable interest in the magnetoplasmadynamic (MPD) arc as a potential spacecraft thruster because of its demonstrated high specific impulse and propulsive efficiency. As a thruster the MPD arc has been studied, both with and without an applied magnetic field, in the low pressure and low propellant mass flow rate regime. A recent critical review of this work can be found in Ref. 1. The MPD arc operating without an applied magnetic field can also be used as a reliable and efficient steady-state source of plasma, and this paper describes in detail the performance of this arc over a range of conditions not previously reported.

With no applied magnetic field the arc was operated at chamber pressures between 26 and 950 torr, argon mass flow rates between 0.08 and 44 g/s and power between 4 and 100 kW. In section A the detailed effects of chamber pressure (at a constant current of 1000 A) on thermal efficiency, arc voltage, energy loss at the electrodes and gas enthalpy are presented and compared with an empirical model. In section B the same type of results, but obtained at constant currents of 200, 400, and 1600 A, are summarized in terms of the same model. In section C the detailed effects of arc current, at several values of argon mass flow rate, on thermal efficiency, arc voltage, total energy loss to the cooled electrodes and stagnation pressure are presented and compared with the same model where applicable. Finally, in section D, the reliability of the arc head is discussed.

II. Experimental Equipment and Procedure

The MPD arc configuration used is shown in Fig. 1, and its schematic in Fig. 2. The water-cooled copper anode had a rounded exit orifice to eliminate erosion due to high head loads in this area. The water-cooled copper face plate, used to attach the arc head to a plenum chamber, was not electrically insulated from the anode; hence, current emission was divided between anode and face plate. The cathode was made of 2% thoriated tungsten. Argon was injected axially into the arc chamber through an annular slit. A bank of rectifiers with peak-to-peak ripple of approximately 3% was used as a power supply. The MPD arc was mounted inside a 2.1-m-diam by 4.2-m long vacuum tank which was exhausted by a 2330 l/s capacity pumping system; hence, the ambient pressure was a function of the argon flow rate. For these experiments the ratio of the arc chamber pressure to vacuum tank pressure was a minimum of 71; therefore, the fluid pressure and temperature inside the electrode region were fixed by the argon flow rate and arc current and were independent of ambient pressure.

Standard calorimetry techniques were used to measure, separately, the heat transfer on the cathode base plate, anode, and face plate. The cooling water flow rate was approximately 0.29 kg/s and was measured with a calibrated turbine flow meter. The coolant temperature rise was measured directly with a calibrated pair of triple-junction thermocouples inserted across each of the three thermal loads. The argon mass flow rate was measured with calibrated rotometers, and the arc chamber and vacuum tank pressures were measured with calibrated strain gauge transducers.

All data was recorded on a Dymec Data System. The estimated maximum uncertainties of each recorded variable are as follows: coolant flow rate ±1%, coolant temperature rise ±0.3%, arc voltage ±0.5%, arc current ±0.5%, pressure ±2%, and mass flow rate ±2%. These estimated uncertainties result in the following errors in the computed quantities: thermal efficiency ±2% at low pressures and ±0.5% at high pressures, total heat transfer rate ±0.02 kW at low heat transfer rates and ±0.14 kW at high rates and gas enthalpy ±4% at low enthalpies and ±5% at high enthalpies.

In this investigation there were only two independent variables, argon mass flow rate and arc current. At each fixed set of variables all information was recorded automatically by the data recording system and then recorded a second time to indicate gross drift in the experiment. The arc current and voltage were also recorded continuously on a strip chart recorder and showed steady values at each fixed mass flow rate and current. The arc was started by simply switching the power supply to the electrodes. This power supply provides 320 Vdc at zero current, and this was sufficient to start the arc with an arc chamber pressure of 10 torr and a mass flow rate of 0.5 g/s. Once the arc was struck, the current and mass flow could be changed throughout their respective ranges without extinguishing the arc.

III. Results and Discussion

A. Effect of Mass Flow Rate on a 1000-A Arc

For this investigation the arc thermal efficiency is based on the dissipated electrical power, as determined from the measured arc voltage, ϕ, and current, I, and the total power picked up by the cooling water, Q_T.

Therefore, the arc thermal efficiency was computed from the following expression:

$$\eta_{TH} \equiv \left(1 - \frac{Q_T}{\phi_I}\right) \times 100 \qquad (1)$$

and is shown as a function of arc chamber pressure, P_c, for a constant current of 1000 A in Fig. 3. The increase of thermal efficiency with increasing chamber pressure can be explained from the known facts that the electric field, E, in the positive column is proportional to $I^m P_c^n$ with $m < 0$ and $n > 0$ (Ref. 2) and that the major power losses from the discharge are approximately independent of gas pressure (Ref. 3), except at very low pressure where they decrease with increasing pressure.

The arc voltage is shown as a function of arc chamber pressure in Fig. 4. Notice that above a pressure of approximately 70 torr the voltage is proportional to P_c^n. To reconcile this experimental result with Ref. 2, in which it was shown both analytically and experimentally that the positive column electric field was proportional to P^n, we must assume that either the anode and cathode falls are small compared to ϕ and that the time-averaged positive column length is independent of pressure, or that the anode and cathode falls are also proportional to P_c^n. Anode falls of from 0.8 to 2.3 V have been measured on a similar arc device,[4] and cathode falls as low as 2 to 3 V for high current arcs with incandescent carbon cathodes are discussed in Ref. 5. Also an anode fall of 1 V was deduced from arc measurements in Ref. 6, and in Refs. 7 and 8 negligibly small anode falls are reported. Notice also, in Fig. 4, a jump of approximately 1 V at a pressure of 138 torr. This behavior occurs occasionally, at any

pressure level, and is usually referred to as a mode change. This change in voltage is not reflected in the heat loss at the electrodes, and it is thought that this mode change represents a change in the positive column. No further explanation of this widely experienced mode change is at present available. In Fig. 3 notice that this voltage jump has a noticeable effect on the thermal efficiency.

The total heat loss from the arc, Q_T, is shown as a function of arc chamber pressure in Fig. 5, and the corresponding relative heat loads on the anode, face plate and cathode base plate are shown in Fig. 6. In Fig. 6 notice that from 94 to 100% of the total heat loss was picked up at the anode and face plate, and Fig. 5 shows that for pressures above approximately 70 torr the heat loss is approximately independent of pressure. This same general behavior of the total and anode heat loss was also found in Ref. 3 over the available argon mass flow range of 0 to 0.8 g/s. The following anode heat-transfer model was proposed and experimentally verified in Ref. 3:

$$Q_A = Q_{CR} + \phi_A I \tag{2}$$

where the total heat input to the anode, Q_A, is given by a term, Q_{CR}, which represents the heat transfer to the anode by convection and radiation plus a term which describes the heat given up to the anode by the collected electron current. This anode heat load due to the electron gas, per unit charge flux, ϕ_A, is defined as

$$\phi_A \equiv \frac{5kT_e}{2e} + \phi_a + \phi_o \tag{3}$$

where the first term represents the enthalpy of the electrons at the sheath edge, the second term is the sheath potential drop or anode fall, and the third term is the material work function.

A plot of the experimentally determined Q_A, or its approximate equivalent Q_T, versus I was found to be a straight line. The term Q_{CR} was then obtained as the ordinate intercept and ϕ_A as the slope of this line. The results obtained in this way[3] show Q_{CR} and ϕ_A to be only weakly dependent on current and pressure and that Q_{CR} was but a few hundred watts. The results obtained in this investigation, over a much wider range of mass flow rate and current, confirm the findings of Ref. 3. These results will be discussed below. For current values of several hundred amperes and above, Q_{CR} is an insignificant part of the total anode heat load and can be disregarded with little error. Therefore, for all but the very lowest currents and pressures, we can take the arc heat losses to be independent of pressure and linearly dependent on current.

Combining the above results for the effects of pressure and current on the arc voltage and heat loss we obtain the following expression for the arc thermal efficiency:

$$\eta_{TH} = \left(1 - \frac{\phi_A}{CP_c^n}\right) \times 100 \qquad (4)$$

where C is a constant of proportionality in this constant current example; however, in general, C contains the effect of current on arc voltage also. The thermal efficiency, computed from Eq. (4), is shown in Fig. 3, which shows a good agreement with the measurements. To make this computation, ϕ_A was obtained from Eq. (2) by neglecting the term Q_{CR} and using

for Q_A an average value of 7.3 kW obtained from Fig. 5 for pressures above 70 torr. If individual values of the heat loss Q_A were used to calculate ϕ_A instead of an average Q_A, the agreement between the calculated and measured thermal efficiency in Fig. 3 would be closer; however, this amount of detail does not appear justified. Also for this constant current experiment the constants C and n were determined from Fig. 4, for pressures above 138 torr, and were found to be 2.74 and 0.387, respectively. For pressures between 70 and 138 torr, n would be the same but C would be slightly less, to account for the mode change. From the results of Ref. 2 we calculate a value of 0.368 for n which agrees very well with our experimentally determined value.

Below an arc chamber pressure of approximately 70 torr the arc voltage lies above the P^n line in Fig. 4 and increases slightly as the pressure is reduced. Also, in Fig. 5, it can be seen that the heat loss increases with decreasing pressure below approximately 70 torr. Based on the anode heat loss model described by Eqs. (2) and (3), it can be concluded that both increases are due to an increased sheath potential drop. Assuming an electron temperature of order 1 V and a work function for the copper anode of 4.4 V the sheath drop increases from an average of 0.4 V at high pressure to 3.9 V at the minimum pressure. This total increase of 3.5 V agrees with the difference between the measured arc voltage and that given by the P^n line in Fig. 4, which is 4.1 V at the minimum pressure. This same effect was noted in Ref. 3 where it was found that both effective anode drop ϕ_A and arc voltage were proportional to P^{-1} for pressures between 20 and 100 torr at zero mass flow rate.

The arc chamber pressure, P_c, and the vacuum tank pressure, P_V, are shown in Fig. 7 as functions of the argon mass flow rate. The non-linear character of the arc chamber pressure at low mass flow rate is caused by a rapidly decreasing stagnation temperature with increasing mass flow rate. This can be seen by writing the one-dimensional fluid continuity equation at the sonic point and differentiating,

$$\frac{dP_t^*}{dm} \propto \frac{\left(T_t^*\right)^{1/2}}{A_s} \tag{5}$$

where P_t^* and T_t^* refer to stagnation conditions at the sonic point, and A_s is the area of the sonic surface which, in general, is only approximately constant. The rapid decrease of stagnation temperature, at low mass flow rate, can be inferred from the enthalpy of the gas which is shown as a function of the arc chamber pressure in Fig. 8. Note that the range of enthalpy shown in Fig. 8 implies an ultimate exhaust velocity in the range of 10^5 to 5×10^5 cm/s. These results suggest that a large part of the total energy is added to the gas upstream of the sonic point and, since the sonic point must lie somewhere in the divergent part of the electrode geometry, that only part of the current is blown far downstream of the arc head. That the arc was, to some extent, blown downstream with increasing mass flow rate can be inferred from the relative heat losses shown in Fig. 6. It can be seen that as the mass flow increased the heat load on the anode decreased, with a corresponding increase in the face plate heat load. The decrease in cathode base plate heat loss could be due to more effective convective cooling of the cathode cylinder at high mass flow rate.

Included in Fig. 8 is the gas enthalpy calculated from the following expression:

$$H = \frac{I\left(CP_c^n - \phi_A\right)}{\dot{m}} + H_{inlet} \qquad (6)$$

where $\dot{m}$ was obtained from a faired line through the data of Fig. 7, and H_{inlet} is the gas enthalpy at the arc inlet.

B. Effect of Mass Flow Rate at Other Currents

The same measurements were also made at a constant arc current of 200, 400 and 1600 A as well as one repeat experiment at 1000 A. The results from these experiments, as well as those of the experiment discussed above, are summarized in Table 1. The thermal efficiency is not predicted as well at 200 and 400 A as it was in Fig. 3 for 1000 A. As an example, at maximum mass flow rate, the predicted thermal efficiency at 200 A was 85.5%, whereas the measured value was 90.2% and at 400 A the predicted value was 78.8% and the measured value 82.5%. The primary reason for these discrepancies was that the variation of total heat loss with arc chamber pressure was relatively greater at the lower currents; hence the use of an average value of Q_T to calculate ϕ_A introduces larger errors. For example, at 1000 A, Q_T varies by ±5% of its average value, while at 200 A the variation is ±35%. When actual values of Q_T are used, the agreement between predicted and measured η_{TH} was again very good. At 1600 A the thermal efficiency is predicted well by the constants in Table 1 for pressures above 130 torr; however, below this pressure, the measured thermal efficiency is under-predicted by as much as 20%. The primary

reason for this discrepancy is that the arc voltage is not represented well by the expression CP^n. For this case the constants of Table 1 were obtained from an average line drawn through the data for pressures of 130 torr and above. Below this pressure the voltage was approximately constant at 14.5 V. It was found that the following empirical expression was a much better fit to the data above 130 torr:

$$\phi = 10.8 + 0.0346\ P_c \tag{7}$$

By using Eq. (7) in Eq. (1) a very good fit to the measured thermal efficiency is obtained for all pressures above 50 torr.

The arc chamber pressures at which the total heat loss reaches its first minimum, 70 torr for the experiment shown in Fig. 5, are also listed in Table 1 as P_{cr}. It was again found that the arc voltage begins to deviate from the expression CP^n at approximately these listed pressures.

C. Effect of Current at Constant Mass Flow Rate

The effect of current on arc head performance was obtained by holding the argon mass flow rate constant at 10 discrete values, between 0.49 and 44.15 g/s, and varying the current in increments at each mass flow rate. The resulting thermal efficiency is shown in Fig. 9 as a function of arc current with mass flow rate as parameter. Only 5 of the 10 distributions are shown for clarity; however, these 5 sets of data are fully representative of the complete set. The corresponding total heat lost to the cooling water and arc voltage are shown in Figs. 10 and 11, respectively. By applying Eq. (2) to the data of Fig. 10, it can be seen that Q_{CR} is at most 400 W and is dependent on the mass flow rate or arc chamber pressure and that ϕ_A is independent of current and approximately independent of mass flow

rate except at the very lowest flow rate. All 10 values of Q_{CR} and ϕ_A are listed in Table 2. The fact that Q_{CR} becomes negative at high mass flow rate cannot be explained by the model leading to Eq. (2); however, considering the gross nature of the model, this is not surprising. Also note the similarity between the variations of thermal efficiency in Fig. 9 and that of voltage in Fig. 11. Again it can be concluded that the thermal efficiency is mainly influenced by the arc voltage over a wide range of current and pressure.

The voltage/current characteristics of Fig. 11 are seen to have a negative slope at low mass flow rate which is normal for free burning arcs. However, at the higher mass flow rates the characteristics become positive over various current ranges. This behavior is typical of constricted arcs in which the cooled confining walls play an important part in removing energy from the positive column. A qualitative view of these characteristics can be obtained from Ref. 9 where the total electrical energy dissipated per unit length of arc column, EI, is equated to the energy loss per unit length. In Ref. 9 the losses are attributed mainly to radiation and thermal conduction radially out of the column. For an assumed radial temperature profile of

$$T(r) = T_{CL}\left[\left(\frac{r}{R}\right)^2 + 1\right]^{-1} \tag{8}$$

they obtain for the column electric field

$$E = I^{-1}\left[Q_R + \pi\lambda T_{CL}\right] \tag{9}$$

In Eqs. (8) and (9) T_{CL} is the column centerline temperature, R the column radius, Q_R the radiation heat loss and λ the thermal conductivity at $r = R$.

At low pressure and current the radiation loss is small, and the energy loss is primarily by conduction out of the column, which is then carried away by forced convection in the present experiments. Since the arc centerline temperature increases slowly with current, the electric field is still proportional to I^m where $-1 < m < 0$. This results in the typical negative arc characteristic. At high pressure and current the radiation loss term, Q_R, becomes important and because of the addition of this term the slope dE/dI increases and can become positive. This effect can clearly be seen in Fig. 11 at mass flow rates of 14.20 and 23.43 g/s. At the highest mass flow rate used, the radiation loss seems to be important even at the low current values.

One other possible cause of the positive arc characteristic, discussed in Ref. 10, is that as the current increases, the pressure in the arc also increases. For the present experiments this pressure rise with current, shown in Fig. 12, is seen to be too small to account for the characteristics of Fig. 11. At the highest mass flow rate used, the arc chamber pressure was not measured because of limitations of the instrumentation then being used. However, from previous experiments, it is known that the pressure at that mass flow rate was approximately 950 torr at a current of 1000 A.

Based on the results of Ref. 2 and of this investigation we will assume that when the energy loss from the positive column is primarily by conduction the arc voltage is given by the following expression:

$$\phi = C_o I^m P_c^n \tag{10}$$

Cross plotting between characteristics, such as those of Figs. 11 and 12, was then used to compute values of n at constant arc current from

$$n = \frac{d \ln \phi}{d \ln P_c} \tag{11}$$

and m was computed from the arc characteristics by using the following expression:

$$m = \frac{d \ln \left(\frac{\phi}{P_c^n} \right)}{d \ln I} \tag{12}$$

The constant C_o could then be obtained from Eq. (10). Only data obtained at low mass flow rates could be used, since at high flow rates the characteristics are distorted by radiation losses. The resulting values of n are shown in Fig. 13 as a function of arc current. The data from Table 1 is also plotted and shows good correspondence with the present experiment. Values of m were obtained for the four lowest mass flow rates by using for n an average value of 0.35 and are listed in Table 2. To compute the constant C_o the average value of -0.235 for m was used. These results are also listed in Table 2. The values of C_o for mass flow rates of 10.65 and 14.20 g/s were obtained from data at the minimum current where the distortion should be the least; however, since the average value of -0.235 for m is not applicable to these distorted characteristics, the values listed are questionable. The fact that at minimum mass flow rate C_o is exceptionally high is probably due to the increased anode sheath drop as was discussed above. The cross-plotted data used to find the values of n shown in Fig. 13 was also used to compute values of C_o. These 12 values of C_o varied between 16.70 and 17.31 with an average value of 16.93.

By using the average values for n and m and values of C_o from Table 2, three characteristics were calculated, corresponding to three measured characteristics, and are shown as the solid lines in Fig. 11. At the two lowest mass flow rates the model and empirical constants are seen to represent the measurements fairly well. The characteristic for a mass flow rate of 14.20 g/s is included as an illustration of the idea that the experimental characteristic was distorted by the radiation loss Q_R. These calculated voltages and values of ϕ_A and Q_{CR} from Table 2 were also used to calculate the thermal efficiency and are compared with the measured values for the three lowest mass flow rates in Fig. 9 (solid curves). At the lowest mass flow rate, the small discrepancies between the measured and calculated voltages, shown in Fig. 11, have a large effect on the thermal efficiency because of the low efficiency level. At a mass flow rate of 5.50 g/s the agreement is very good because the voltage errors have less significance at higher thermal efficiency. Of course, at 14.20 g/s the agreement is poor because the assumed radiation loss from the plasma is not taken into account in the definition of thermal efficiency.

D. Reliability

Accumulated running times on the order of 100 h between overhauls, including approximately as many starts and shutdowns, have been noted with regularity. The most common failure, requiring arc head overhaul, has been that of the insulator between the anode and cathode. Insulators made of a polymerized-resin-impregnated linen (Micarta) and the polymerized resin methyl methacrylate (Lucite) ablate. The rate of ablation was probably low.

However, this ablation does result in a gradual buildup of material on the cooled cylindrical surface of the anode. After many hours of operation this buildup reaches local thicknesses of order 1 mm. A spectroscopic analysis showed this material to be 95 to 98% carbon, 2 to 5% tungsten, 0.05% silicon, and minor traces of other metallic impurities. The carbon and silicon must have come from the ablating insulator and the tungsten from the cathode. An anodized aluminum insulator was also tried with success except when the arc was operated at the minimum current and mass flow rate reported here. Under these conditions the arc attaches to the anode far upstream near the insulator. The heat load is then too high and the insulator fails. Currently boron nitride insulators are being used with no apparent problems.

This arc head has also been run over a limited range of conditions with helium and hydrogen as working fluids. The only difficulty experienced with these two gases was a higher heat transfer rate on the rounded exit orifice of the anode. With helium some copper was lost at first but the arc still functioned. However, with hydrogen the heat loads were high enough to cause anode failure after a few minutes of operation.

IV. Conclusions

An MPD arc without applied magnetic field was used to produce a continuous stream of argon plasma over a very wide range of mass flow rate and arc current. From measurements of arc voltage, chamber pressure and heat transfer rates to the electrodes gross operating characteristics have been deduced and from these the following conclusions were obtained:

(1) The arc thermal efficiency is a strong function of chamber pressure but only weakly dependent on current. Efficiencies approaching 90% at pressures of order 1 atm were obtained.

(2) At least 94% of the total energy lost to the cooled electrodes was deposited in the anode and, except at low pressure and current, this energy loss is approximately independent of pressure and linearly dependent on current.

(3) Over most of the operating range tested the arc voltage was proportional to P_c^n, where P_c is the arc chamber pressure and n is a weak function of arc current. However, the voltage was also found to be a complex function of current at intermediate and high pressure.

(4) The MPD arc can be operated without an applied magnetic field and without fluid swirl over the entire range of parameters tested for long periods of time with negligible anode erosion.

(5) The range of mass flow rate and current tested was limited by the gas supply system and power supply available. The data indicates than an extension of these ranges should be possible with no detrimental effects to the MPD arc.

References

[1] Nerheim, N. M., and Kelly, A. J., "A Critical Review of the Magnetoplasmadynamic (MPD) Thruster for Space Applications," Technical Report 32-1196, Jet Propulsion Laboratory, Pasadena, Calif., Feb. 15, 1968.

[2]Suits, C. G., and Poritsky, H., "Application of Heat Transfer Data to Arc Characteristics," Physical Review, Vol. 55, June 15, 1939, p. 1184.

[3]Shih, K. T., Pfender, E., and Eckert, E. R. G., "Thermal Analysis of Cathode and Anode Regimes of an MPD-Arc," Summary Report (HTL TR No. 70), Heat Transfer Laboratory, Mechanical Engineering Dept., University of Minnesota, Minneapolis, Minn., January 1968.

[4]Bose, T. K., Pfender, E., "Direct and Indirect Measurements of the Anode Fall in a Coaxial Arc Configuration," AIAA Journal, Vol. 7, No. 8, Aug. 1969, pp. 1643-1644.

[5]Finkelnburn, W., and Maecker, H., "Electric Arcs and Thermal Plasma," Handbuch der Physik, Vol. XXII, Springer-Verlag, Berlin, 1956.

[6]Eberhart, R. C., and Seban, R. A., "The Energy Balance for a High Current Argon Arc," International Journal of Heat and Mass Transfer, Vol. 9, Pergamon Press, New York, 1966, pp. 939-949.

[7]Fay, J. A., and Hogan, W. T., "Heat Transfer to Cold Electrodes in a Flowing Ionized Gas," The Physics of Fluids, Vol. 5, No. 8, Aug. 1962.

[8]Skolnik, M., and Jones, T. B., "Characteristics of the High Current Tungsten Arc in Argon, Helium, and Their Mixtures," Journal of Applied Physics, Vol. 23, No. 6, June 1952.

[9]Von Engel, A., Ionized Gases, Oxford University Press, New York, 1955.

[10]Cobine, J. D., Gaseous Conductors, Dover Publications, Inc., New York, 1958.

Table 1 Summary of results from constant current experiments

I, A	ϕ_A, V	C	n	P_{cr}, torr
200	7.0	8.94	0.247	26
400	7.9	4.52	0.313	50
1000	7.3	2.74	0.387	70
1000	7.5	3.07	0.392	80
1600	7.4	1.16	0.519	130

Table 2 Summary of results from constant $\dot{m}$ experiments

$\dot{m}$, g/s	m	C_o	ϕ_A, V	Q_{CR}, kW
0.49	-0.248	19.54	8.26	0.38
2.00	-0.221	17.41	7.78	0.30
4.00	-0.253	17.10	7.52	0.34
5.50	-0.218	16.93	7.81	0.22
7.10	--	--	7.64	0.21
10.65	--	(16.16)	7.41	0.11
14.20	--	(15.69)	7.58	0.13
23.43	--	--	7.38	-0.18
32.00	--	--	7.43	-0.40
44.15	--	--	7.40	-0.32

Figures

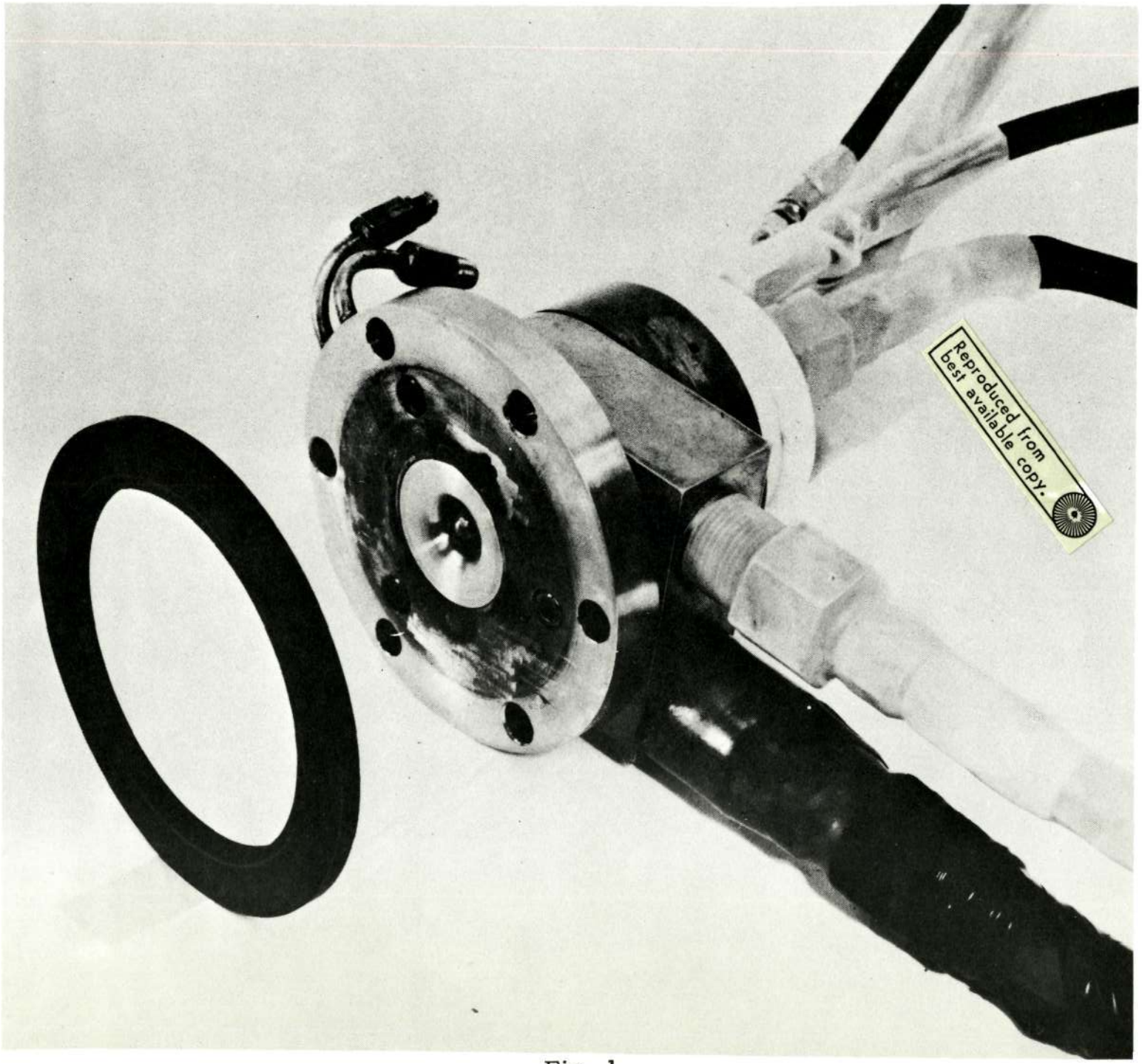

Fig. 1

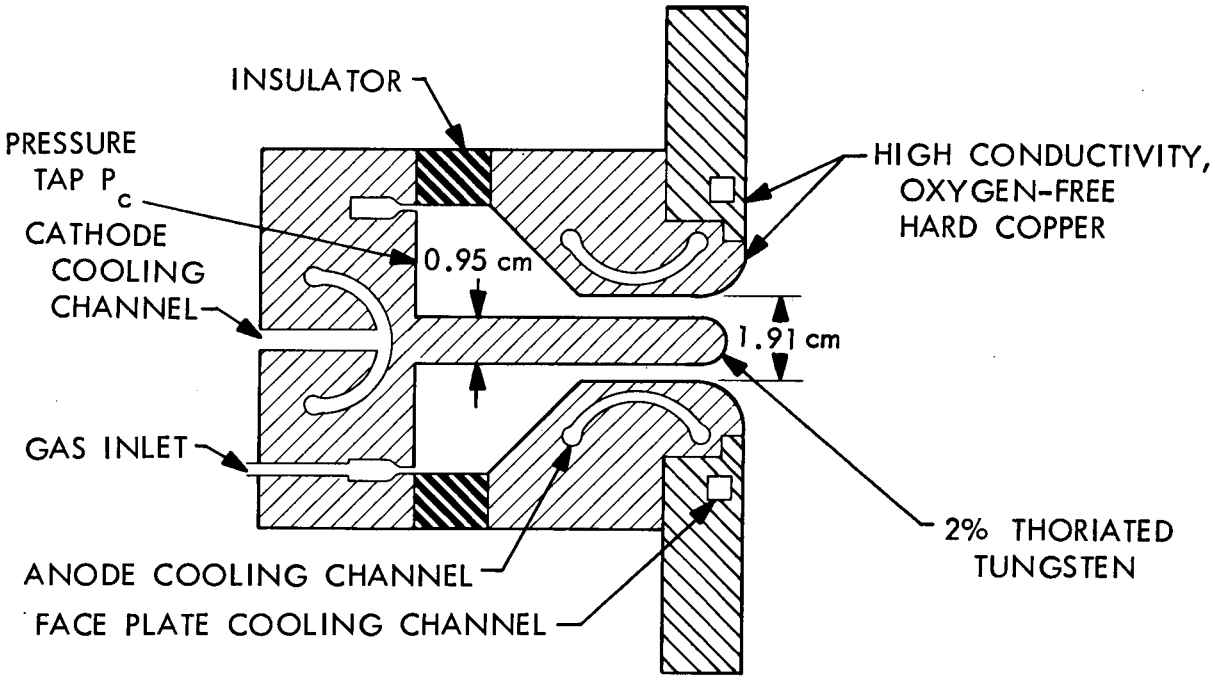
INSULATOR
PRESSURE TAP P_c
CATHODE COOLING CHANNEL
0.95 cm
1.91 cm
HIGH CONDUCTIVITY, OXYGEN-FREE HARD COPPER
GAS INLET
2% THORIATED TUNGSTEN
ANODE COOLING CHANNEL
FACE PLATE COOLING CHANNEL

Fig. 2

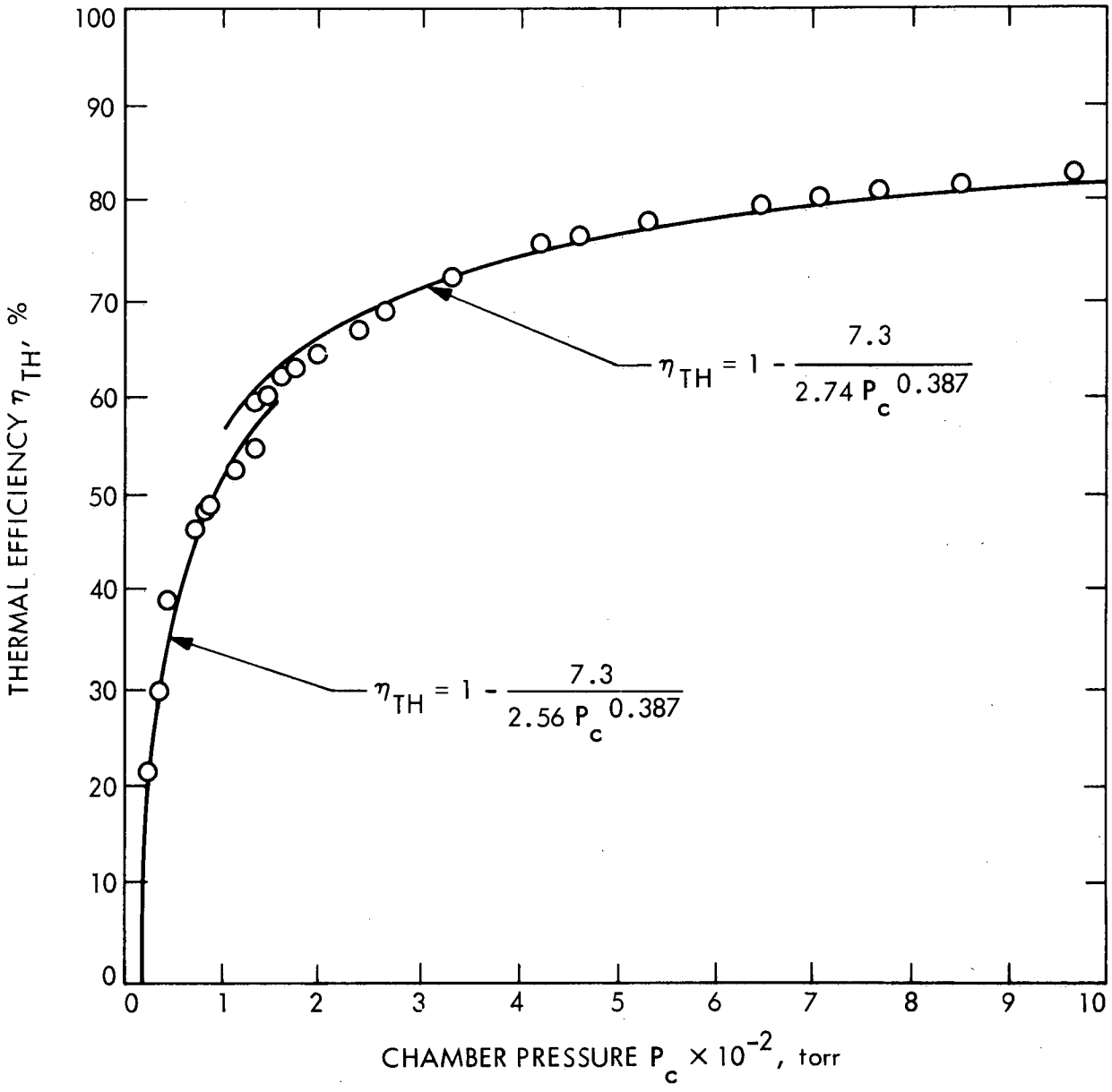
THERMAL EFFICIENCY η_{TH}, %
100
90
80
70
60
50
40
30
20
10
0
0
1
2
3
4
5
6
7
8
9
10
CHAMBER PRESSURE $P_c \times 10^{-2}$, torr
$\eta_{TH} = 1 - \frac{7.3}{2.74\ P_c^{0.387}}$
$\eta_{TH} = 1 - \frac{7.3}{2.56\ P_c^{0.387}}$

Fig. 3

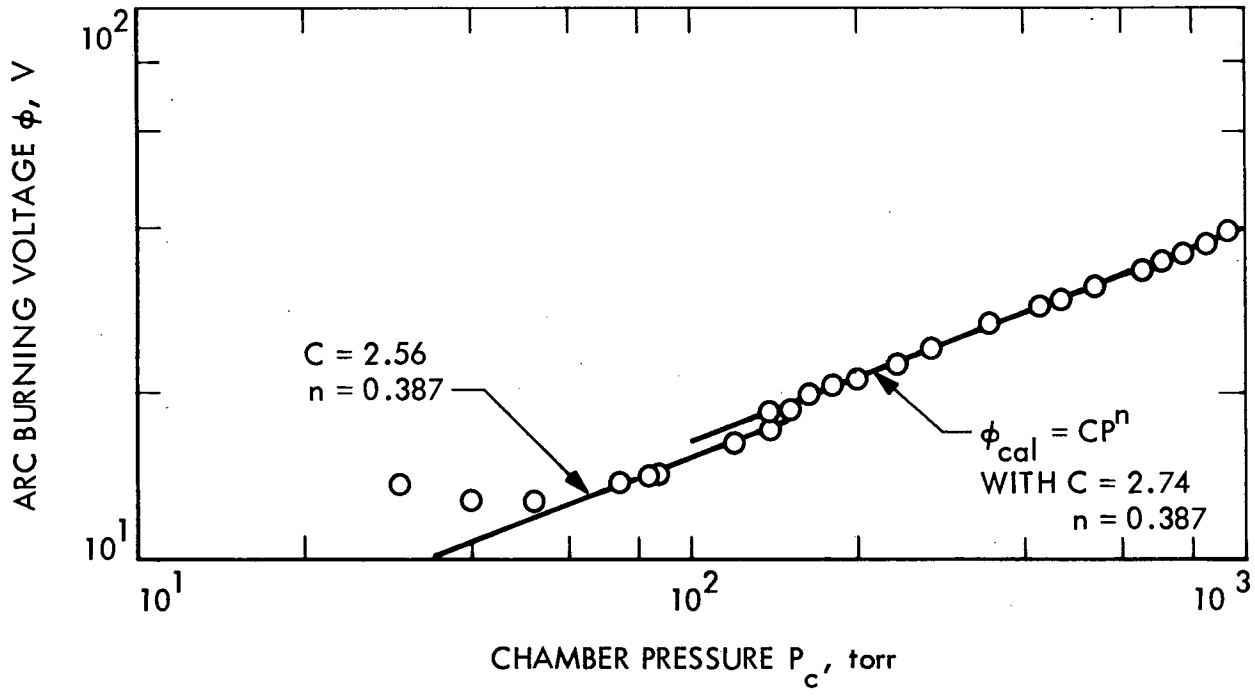
ARC BURNING VOLTAGE φ, V
10^2
10^1
C = 2.56
n = 0.387
$\phi_{cal} = CP^n$
WITH C = 2.74
n = 0.387
10^1
10^2
10^3
CHAMBER PRESSURE P_c, torr

Fig. 4

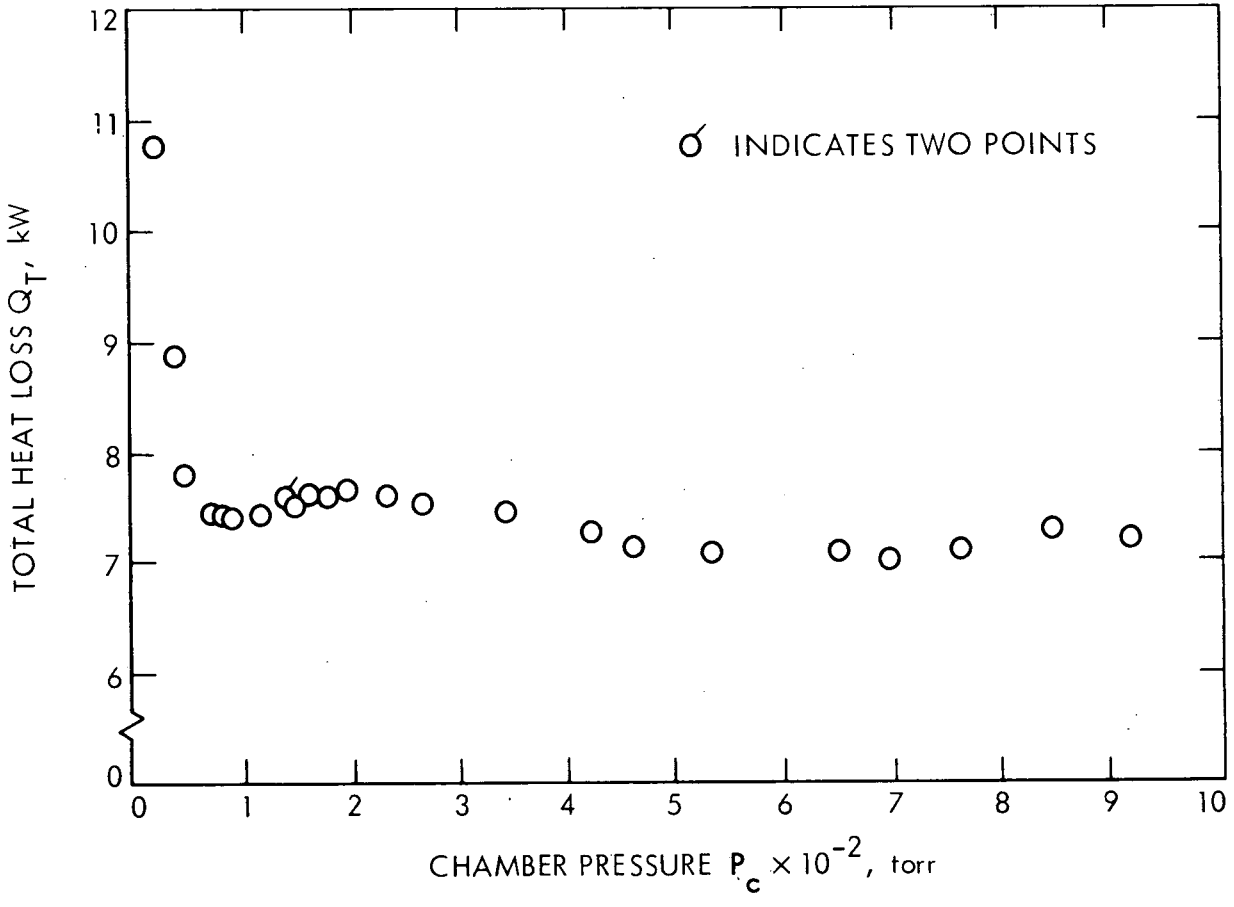
12
11
10
9
8
7
6
0
0
1
2
3
4
5
6
7
8
9
10
INDICATES TWO POINTS
TOTAL HEAT LOSS Q_T, kW
CHAMBER PRESSURE $P_c \times 10^{-2}$, torr

Fig. 5

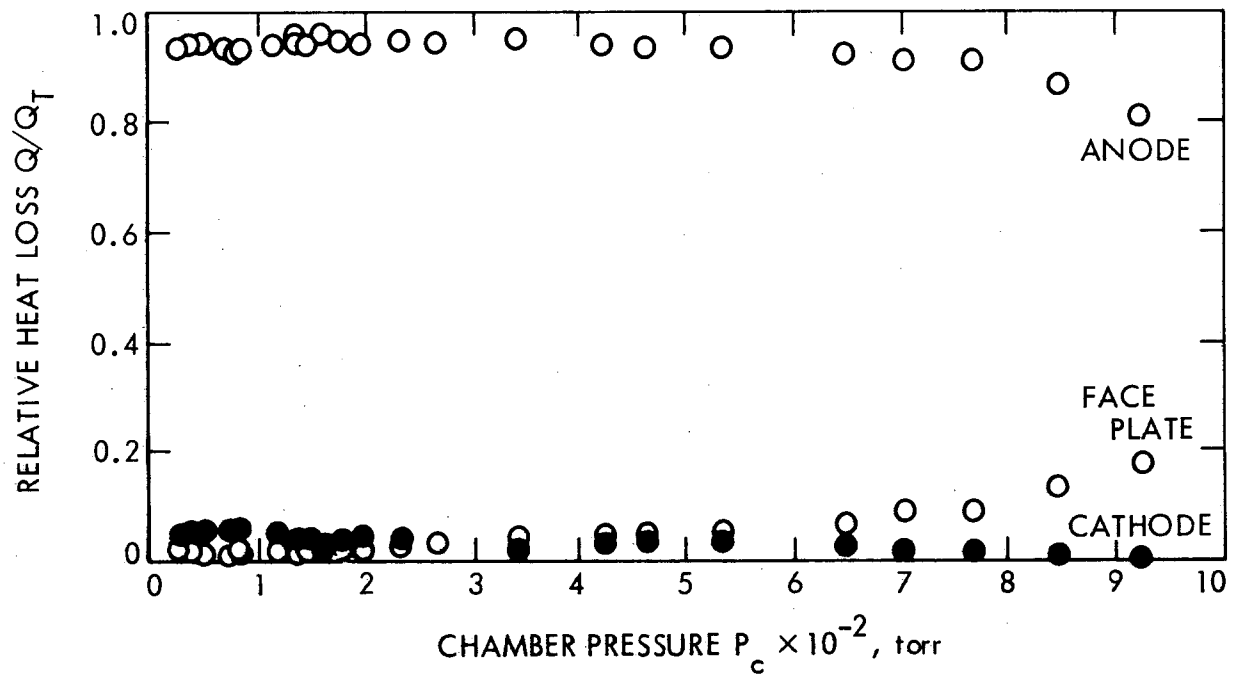
RELATIVE HEAT LOSS Q/Q_T
1.0
0.8
0.6
0.4
0.2
0
0
1
2
3
4
5
6
7
8
9
10
ANODE
FACE
PLATE
CATHODE
CHAMBER PRESSURE P_c × 10^-2, torr

Fig. 6

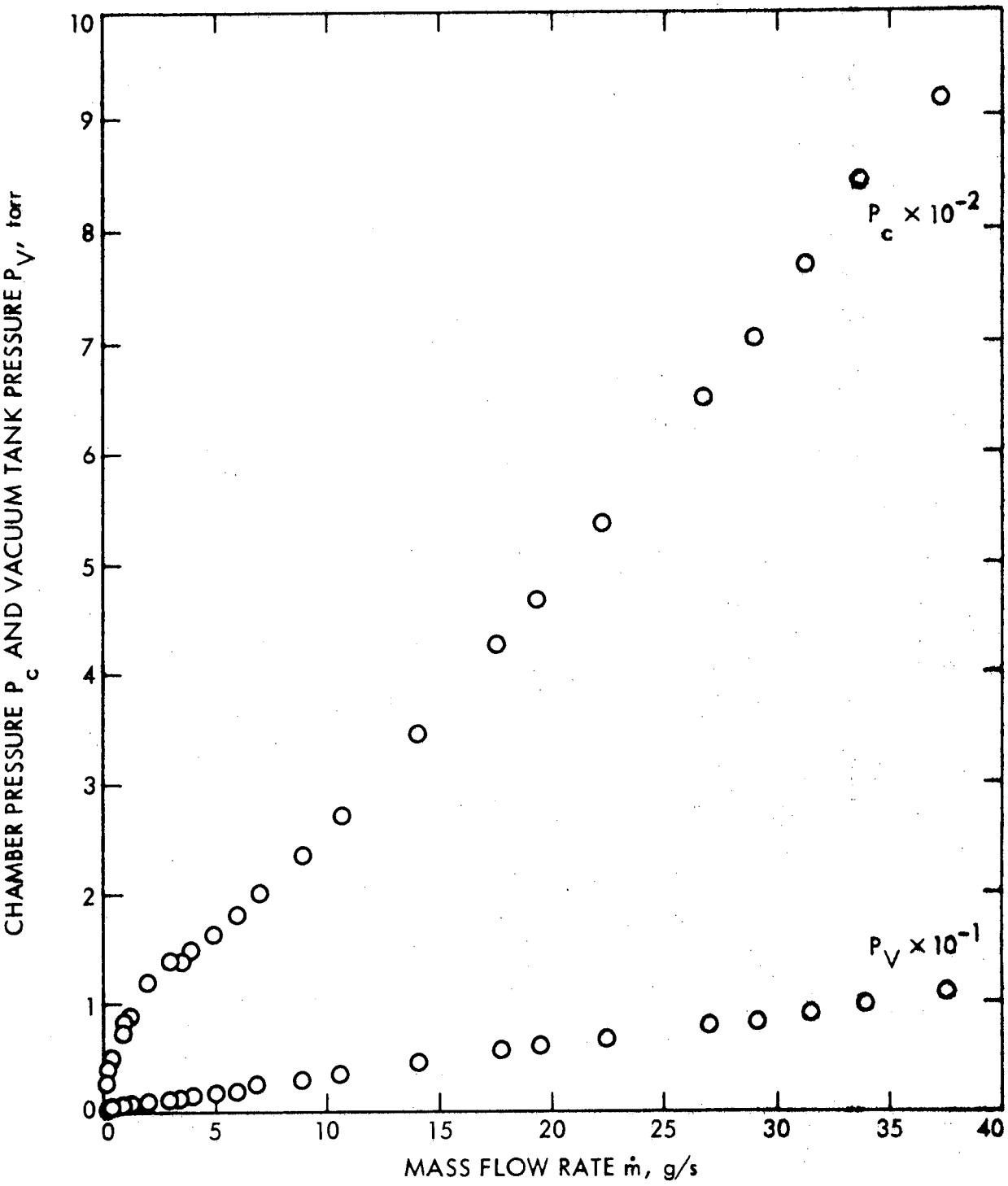
CHAMBER PRESSURE P_c AND VACUUM TANK PRESSURE P_V, torr
MASS FLOW RATE $\dot{m}$, g/s
$P_c \times 10^{-2}$
$P_V \times 10^{-1}$
0
1
2
3
4
5
6
7
8
9
10
0
5
10
15
20
25
30
35
40

Fig. 7

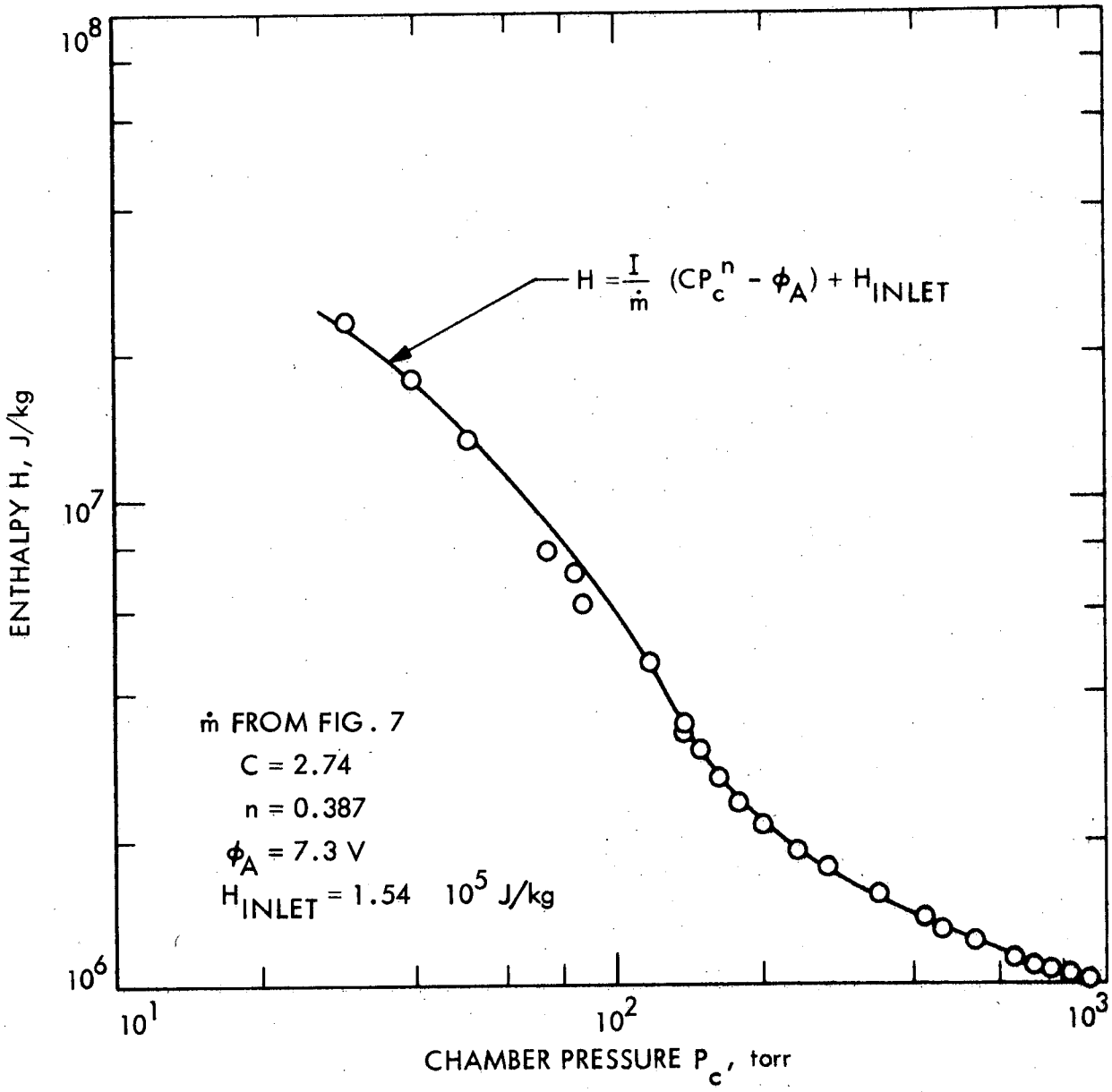
10^8
10^7
10^6
ENTHALPY H, J/kg
$H = \frac{I}{\dot{m}} (CP_c^n - \phi_A) + H_{INLET}$
$\dot{m}$ FROM FIG. 7
C = 2.74
n = 0.387
ϕ_A = 7.3 V
H_{INLET} = 1.54 10^5 J/kg
10^1
10^2
10^3
CHAMBER PRESSURE P_c, torr

Fig. 8

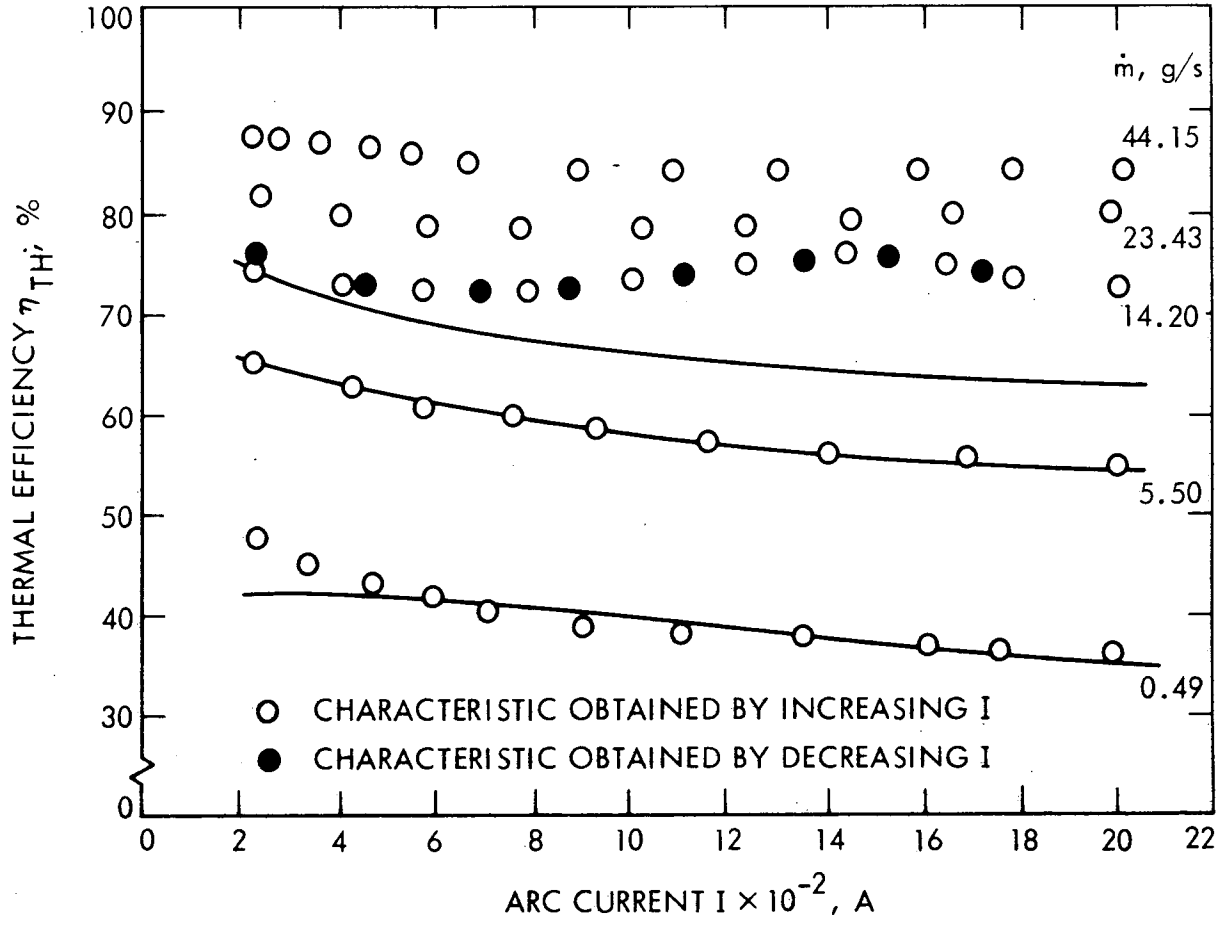
THERMAL EFFICIENCY η_{TH}, %
100
90
80
70
60
50
40
30
0
0
2
4
6
8
10
12
14
16
18
20
22
ARC CURRENT I × 10^{-2}, A
ṁ, g/s
44.15
23.43
14.20
5.50
0.49
CHARACTERISTIC OBTAINED BY INCREASING I
CHARACTERISTIC OBTAINED BY DECREASING I

Fig. 9

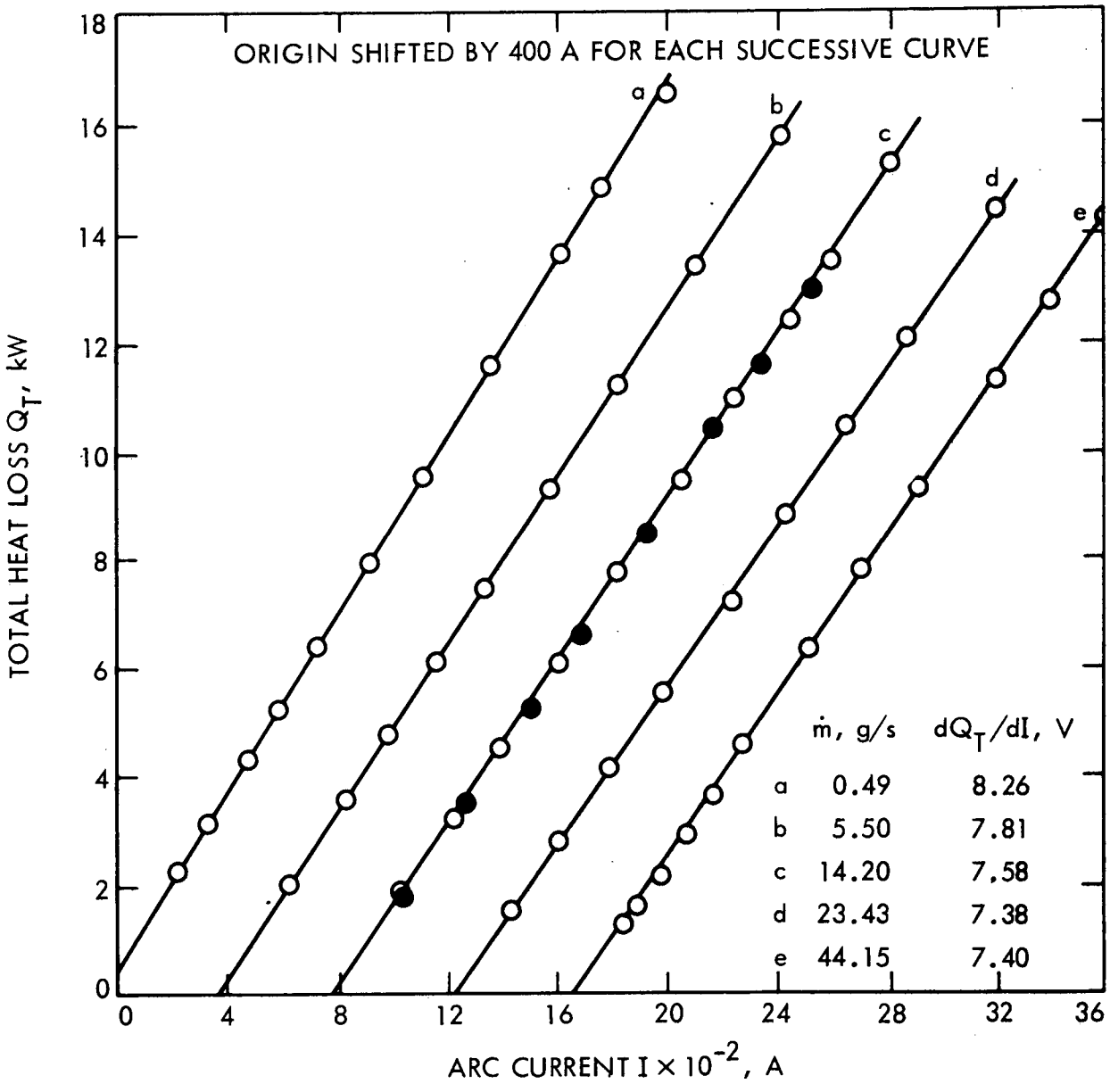
ORIGIN SHIFTED BY 400 A FOR EACH SUCCESSIVE CURVE
TOTAL HEAT LOSS Q_T, kW
ARC CURRENT I × 10^{-2}, A
0
2
4
6
8
10
12
14
16
18
0
4
8
12
16
20
24
28
32
36
a
b
c
d
e
ṁ, g/s
dQ_T/dI, V
a 0.49 8.26
b 5.50 7.81
c 14.20 7.58
d 23.43 7.38
e 44.15 7.40

Fig. 10

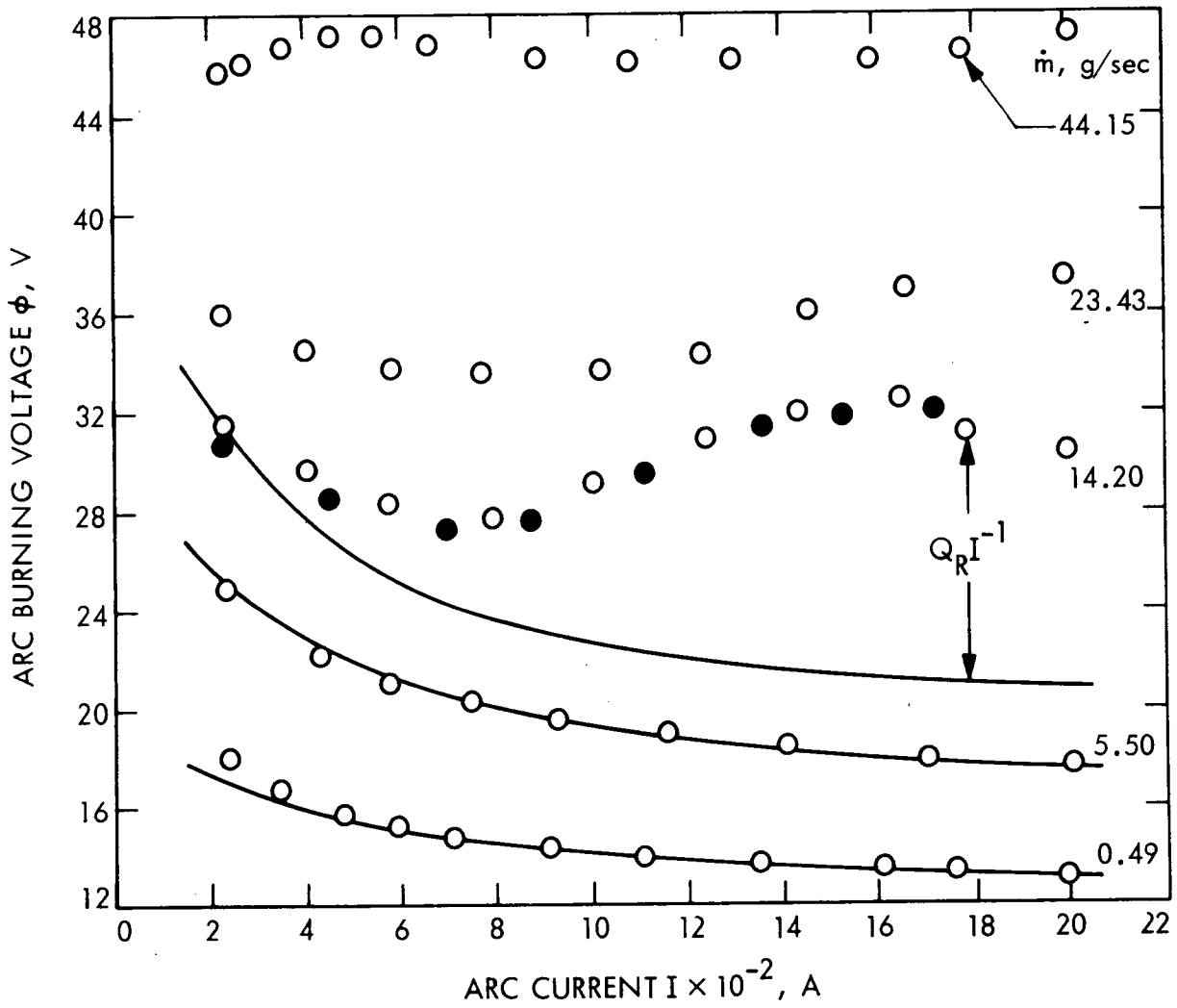
ARC BURNING VOLTAGE ϕ, V
ARC CURRENT I × 10^-2, A
ṁ, g/sec
44.15
23.43
14.20
5.50
0.49
Q_R I^-1
48
44
40
36
32
28
24
20
16
12
0
2
4
6
8
10
12
14
16
18
20
22

Fig. 11

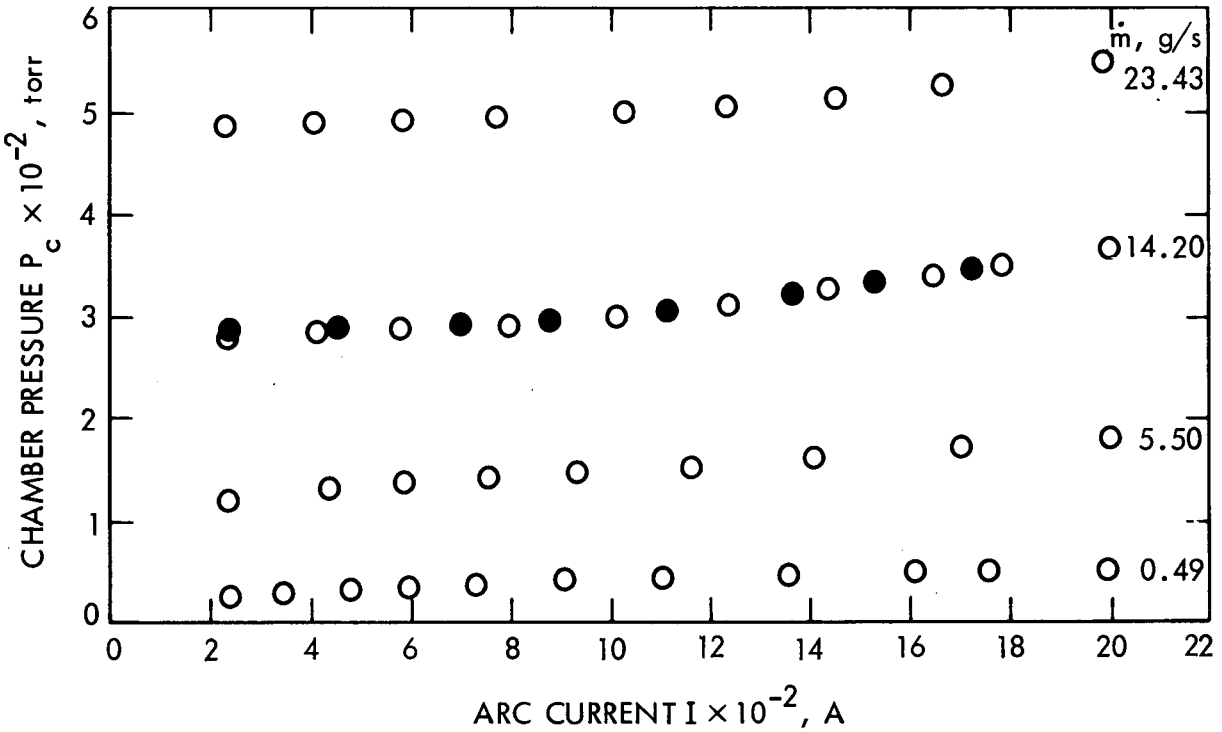
CHAMBER PRESSURE $P_c \times 10^{-2}$, torr
ARC CURRENT I $\times 10^{-2}$, A
$\dot{m}$, g/s
23.43
14.20
5.50
0.49
0
1
2
3
4
5
6
0
2
4
6
8
10
12
14
16
18
20
22

Fig. 12

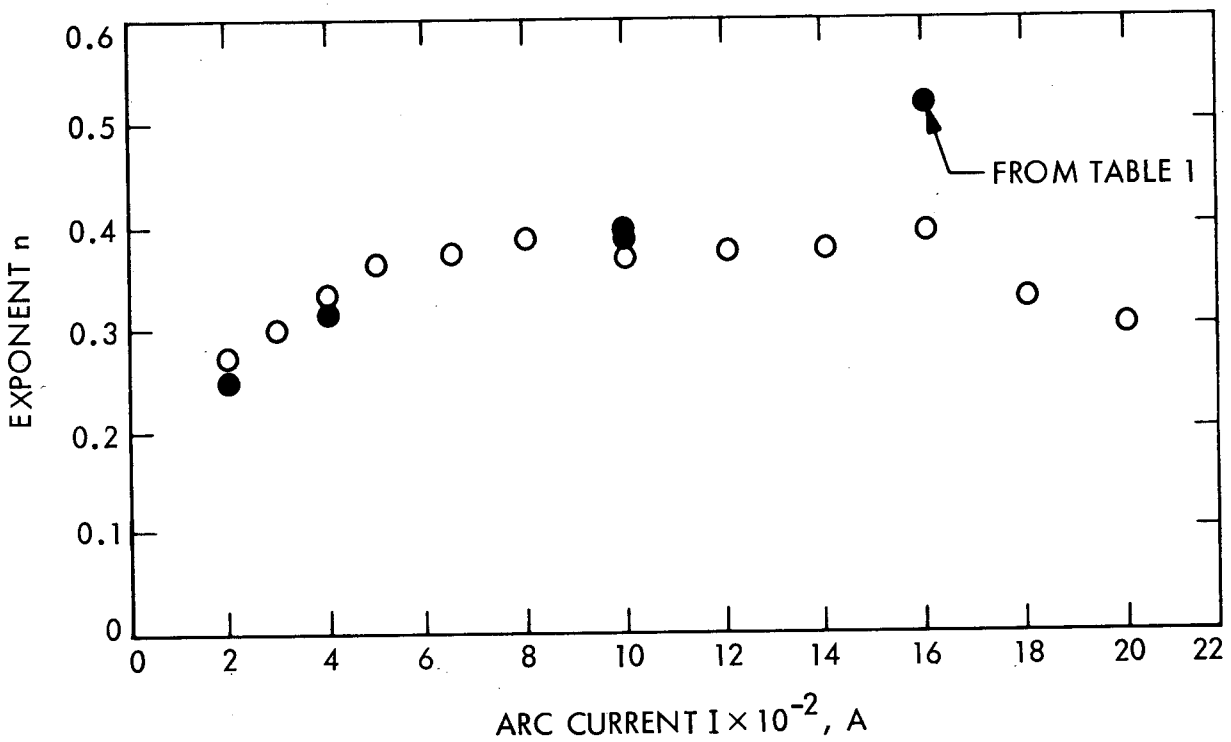
0.6
0.5
0.4
0.3
0.2
0.1
0
EXPONENT n
FROM TABLE 1
0
2
4
6
8
10
12
14
16
18
20
22
ARC CURRENT I × 10^-2, A

Fig. 13